

# Powerful Radio Emission From Low-mass Supermassive Black Holes Favors Disk-like Bulges

J. Wang<sup>1,2</sup>, Y. Xu<sup>1,2</sup>, D. W. Xu<sup>1,2</sup> and J. Y. Wei<sup>1,2</sup>

wj@bao.ac.cn

## ABSTRACT

The origin of spin of low-mass supermassive black hole (SMBH) is still a puzzle at present. We here report a study on the host galaxies of a sample of radio-selected nearby ( $z < 0.05$ ) Seyfert 2 galaxies with a BH mass of  $10^{6-7} M_{\odot}$ . By modeling the SDSS  $r$ -band images of these galaxies through a 2-dimensional bulge+disk decomposition, we identify a new dependence of SMBH's radio power on host bulge surface brightness profile, in which more powerful radio emission comes from a SMBH associated with a more disk-like bulge. This result means low-mass and high-mass SMBHs are spun up by two entirely different modes that correspond to two different evolutionary paths. A low-mass SMBH is spun up by a gas accretion with significant disk-like rotational dynamics of the host galaxy in the secular evolution, while a high-mass one by a BH-BH merger in the merger evolution.

*Subject headings:* galaxies: nuclei - galaxies: bulges - galaxies: Seyfert

## 1. INTRODUCTION

It was for a long time to recognize a remarkable radio-loud/radio-quiet (RL/RQ) dichotomy for active galactic nuclei (AGNs). RL-AGNs prefer to be associated with high-mass supermassive black holes (SMBHs), i.e.,  $M_{\text{BH}} > 10^8 M_{\odot}$  (e.g., Laor 2000). While, a very wide range of  $M_{\text{BH}}$  can be found for RQ-AGNs. The RL/RQ dichotomy is, however, challenged

---

<sup>1</sup>CAS Key Laboratory of Space Astronomy and Technology, National Astronomical Observatories, Chinese Academy of Sciences

<sup>2</sup>School of Astronomy and Space Science, University of Chinese Academy of Sciences

by the identification of dozens of RL narrow-line Seyfert 1 galaxies (e.g., Komossa et al. 2006). The special observational properties of NLS1s enable most of authors believe that they are the objects at early evolutionary phase associated with low-mass SMBH and very high Eddington ratio (e.g., Mathur 2000; Zhou et al. 2006).

BH’s spin is widely believed to play a crucial role in determining the radio emission from SMBHs. A scenario that an energy extraction from a SMBH spun up by a BH-BH merger (e.g., Chiaberge & Marconi 2011) is favored for high-mass SMBHs. This spin-up scenario is, however, almost infeasible for low-mass SMBHs, because they are believed to largely build from secular evolution driven by internal dynamical processes in the disk growth rather than from a merge of two BHs (e.g., Kormendy & Ho 2013).

The origin of angular momentum of these low-mass SMBHs is therefore still a puzzle at present. In this paper, we attempt to address the puzzle from a different perspective based on the properties of the host galaxy that can provide a clue of evolutionary information through stellar dynamics and population. This aim naturally requires us to focus on radio-selected type II AGNs with small  $M_{\text{BH}}$  in stead of their type I counterparts, because the obscuration of the central bright nuclei by the dust torus allows the stellar population and morphology of the host galaxies to be easily measured from ground observations for the type II AGNs. In a type I AGN, its host galaxy is typically overwhelmed by the AGN’s continuum and broad lines in optical wavelengths.

The paper is organized as follows. The sample selection and image analysis are described in §2 and 3, respectively. The statistical results along with the implications are shown in §4. A  $\Lambda$ CDM cosmology with parameters  $H_0 = 70 \text{ km s}^{-1} \text{ Mpc}^{-1}$ ,  $\Omega_{\text{m}} = 0.3$ , and  $\Omega_{\Lambda} = 0.7$  is adopted throughout the paper.

## 2. SAMPLE SELECTION: SDSS/FIRST NEARBY SEYFERT 2 GALAXIES WITH SMALL BLACK HOLE MASS

A sample of radio-selected nearby Seyfert 2 galaxies with small  $M_{\text{BH}}$  is selected as follows.

### 2.1. Seyfert 2 Galaxies with Small $M_{\text{BH}}$

We start from the value-added SDSS Data Release 7 Max-Planck Institute for Astrophysics/Johns Hopkins University (MPA/JHU) catalog (see Heckman & Kauffmann 2006 for a review). At the beginning, we require the objects with a redshift smaller than 0.05 to

ensure their host galaxies can be resolved by the SDSS image observations. Given the line fluxes reported in the catalog, we then extract “pure” Seyfert 2 galaxies from the selected low- $z$  objects by using a series of demarcation schemes (Kewley et al. 2001, 2006) based on the widely used three Baldwin-Phillips-Terlevich diagnostic diagrams (e.g., Veilleux & Osterbrock 1987). To further avoid the contamination by low-ionization nuclear emission regions (LINERs), we require the  $[\text{O III}]/[\text{O II}]$  line ratio<sup>1</sup> is larger than 3 according to the scheme proposed by Heckman et al. (1981).

Objects with small  $M_{\text{BH}}$  are then extracted from the selected “pure” Seyfert 2 galaxies according to the well-documented  $M_{\text{BH}}-\sigma_*$  relationship (e.g., Magorrian et al. 1998). The values of velocity dispersion  $\sigma_*$  of the star component are taken from the MPA/JHU catalog. The objects with measured  $\sigma_*$  between 80 and 120 km s<sup>−1</sup> are retained in our subsequent sample selection. This range of  $\sigma_*$  corresponds to a  $M_{\text{BH}}$  of  $10^{6-7} M_{\odot}$ , based the recent calibration of  $\log(M_{\text{BH}}/M_{\odot}) = (8.32 \pm 0.05) + (5.64 \pm 0.32) \log(\sigma_*/200 \text{ km s}^{-1})$  presented in McConnell & Ma (2013). The calibration is valid for a sample of  $M_{\text{BH}}$  of  $10^{6-10} M_{\odot}$ . The lower limit of  $\sigma_* = 80 \text{ km s}^{-1}$  is used in our sample selection because of the instrumental spectral resolution of SDSS of  $\sim 70 \text{ km s}^{-1}$ .

## 2.2. Cross-match with First Survey

The selected “pure” Seyfert 2 galaxies with small  $M_{\text{BH}}$  are subsequently cross-matched with the FIRST survey catalog (Becker et al. 2003). The cross-match follows the methods described in Richards et al (2002), in which a matching radius of  $2''$  is adopted for compact radio sources, and a radius of  $6'$  for possible extended sources<sup>2</sup>. With the FIRST limiting flux density ( $5\sigma$ ) of 1 mJy, our cross-match finally returns 54 radio-selected Seyfert 2 galaxies with small  $M_{\text{BH}}$ .

The radio power at 1.4 GHz (rest frame) of each of the 54 selected objects is calculated from the observed integrated flux density  $f_{\nu}$  through the formula  $P_{1.4\text{GHz}} = 4\pi d_L^2 f_{\nu} (1+z)^{-1-\alpha}$ , where  $d_L$  is the luminosity distance,  $z$  the redshift, and  $\alpha = -0.8$  (e.g., Ker et al. 2012) the spectral slope defined as  $f_{\nu} \propto \nu^{\alpha}$ . The derived  $P_{1.4\text{GHz}}$  has a range from  $10^{21}$  to

---

<sup>1</sup>A correction of local extinction is applied to the observed line fluxes by a combination of a Balmer decrement for the standard case B recombination and a Galactic extinction curve with  $R_V = 3.1$  throughout the paper.

<sup>2</sup>At  $z = 0.01$ , the radius of  $6'$  corresponds to a physical size of  $\sim 70 \text{ kpc}$  that is close to the size ( $\sim 100 \text{ kpc}$ ) of typical jets and lobes. In fact, all the objects listed in our final sample have redshifts larger than 0.01 (see Table 1).

$10^{23} \text{W Hz}^{-1}$ . We estimate the radio loudness of each object by using the [O III] luminosity  $L_{[\text{OIII}]}$  as a proxy of AGN’s bolometric luminosity  $L_{\text{bol}}$ . The combination of the widely used bolometric corrections of  $L_{\text{bol}} \approx 3500 L_{[\text{OIII}]}$  and  $L_{\text{bol}} = 9 \lambda L_{\lambda}(5100 \text{\AA})$  (Heckman & Best 2014; Kaspi et al. 2000) leads to an estimation of radio loudness  $R'$ <sup>3</sup>

$$\log R' = \log \left( \frac{P_{1.4\text{GHz}} / \text{W Hz}^{-1}}{L_{[\text{OIII}]} / \text{erg s}^{-1}} \right) + 19.18 \quad (1)$$

It must be stressed that the possible systematics of the used bolometric corrections mean that the derived  $R'$  is only meaningful for a comparison study.

### 2.3. Sample Selection on AGN’s Activity

The aim of this study is to explore the effect of host galaxy on the origin of radio emission in AGNs, which requires a sample selected on nuclear accretion property. Figure 1 shows an anti-correlation between the calculated  $L_{[\text{OIII}]}$  and  $R'$  for all the selected 54 objects. The anti-correlation motivates us to exclude the objects at the right-bottom (left-top) corner for the current study, because the most large (small)  $R'$  of these objects are simply caused by their extremely low (high) accretion activities rather than powerful (weak) radio emission. With these considerations, we finally focus on the objects located within a bin of  $\log L_{[\text{OIII}]} = 40.6 - 41.2$ . The bin size is chosen by a compromise between the scatter of the  $L_{[\text{OIII}]}$  versus  $R'$  correlation and the size of our finally used sample.

In summary, we finally selected 31 radio-selected nearby ( $z < 0.05$ ) Seyfert 2 galaxies with small  $M_{\text{BH}}$  of  $10^{6-7} M_{\odot}$ , after removing the duplications. The properties of these objects are listed in Table 1, except for SDSS J160151.51+024809.9 (see Section 3 for the details).

## 3. DATA REDUCTIONS: TWO-DIMENSIONAL BULGE/DISK DECOMPOSITION

At first, the SEXTRACTOR package (Bertin & Arnouts 1996) is performed for each of the SDSS-corrected  $r$ -band frames to determine the detection threshold, and to define the area where the galaxy signal is above the determined threshold. A threshold of 1.5 times of the background noise is adopted in our data reduction. A stamp image centered on the object

---

<sup>3</sup> Assuming an universal spectral slope of  $\alpha = -0.8$  yields a transformation of  $R'_{1.4\text{GHz}} = 2.77 R_{5\text{GHz}}$ . The tiny difference between the monochromatic optical luminosities at 4400Å and 5100Å is ignored in our study.

is therefore produced by the SEXTRACTOR package. With the stamp images, we perform a 2-dimensional bulge+disk decomposition by the publicly available GIM2D package<sup>4</sup> (Simard et al. 2002) that is demonstrated to be valid for different galaxy samples (e.g., de Jong et al. 2004), except for SDSS J160151.51+024809.9. The image shows that the host of the object is a heavily obscured edge-on disk galaxy. The surface brightness profile used in our decomposition is described by a combination of an exponential radial profile for the disk component and a Sersic profile with an index of  $n_B$  for the bulge component. A simple point spread function (PSF) with a Gaussian profile is adopted in the convolution of our modeling to account for the seeing effect. The resulted reduced  $\chi^2$  is very close to unit for all the 30 host galaxies.

Table 1 tabulates some modeled parameters of the 30 host galaxies. The parameters are B/T ratio, the ratio of the disk scale length over the bulge effective radius  $h_d/r_e$  and the Sersic index  $n_B$ . The reported uncertainties given by the GIM2D package at a confidence level of 99% are based on the topology of the parameter space being built up in the fitting.

## 4. RESULTS AND IMPLICATIONS

Two objects (SDSS J154559.09+270629.5 and SDSS J162622.65+210542.8) are excluded from subsequent statistical analysis because their modeled bulge effective radius  $r_e$  are extremely smaller than the size of the corresponding PSF.

### 4.1. Statistical Results

The modeled  $n_B$  is plotted against the calculated  $R'$ ,  $L_{[\text{OIII}]}$ , and  $P_{1.4\text{GHz}}$  in the left, middle and right panels in Figure 5, respectively. The left panel shows a newly identified anti-correlation between  $R'$  and  $n_B$ . In fact, the galaxies with  $R' < 1$  generally tend to have a classical bulge with  $n_B > 2.0$ , while the ones with  $R' > 1$  a pseudo-bulge with  $n_B < 2.0$  (e.g., Kormendy & Kennicutt 2004; Fisher & Drory 2008). A Spearman rank-order statistical test yields a correlation coefficient of  $r_s = -0.54$ . The corresponding probability of null correlation from two-tailed is calculated to be  $p_s = 0.0029$ , which corresponds to a significant level at  $2.81\sigma$ . As an additional test, a generalized Kendall's  $\tau$  correlation coefficient is calculated to be  $\tau = -0.78$  at a significance level of  $2.91\sigma$ . The corresponding probability of null correlation is inferred to be  $p_s = 0.0037$ . A comparison of the plots in

---

<sup>4</sup>The home page of the GIM2D package can be found at <http://astrowww.phys.uvic.ca/~simard/GIM2D/>.

the middle and right panels clearly shows that it is the radio power, rather than the AGN’s accretion activity, depending on the modeled  $n_B$ .

Figure 6 plots  $R'$  against various properties of host galaxy. At first, one can see from the plot that there is an independence of  $R'$  on the stellar population age as assessed by the parameter  $D_n(4000)$ , although almost all the host galaxies are associated with relatively young stellar populations, i.e.,  $D_n(4000) < 1.6$  (e.g., Heckman & Best 2014). Another independence can be identified for  $R'$  on the measured bulge fraction B/T, which implies that the radio emission from the low-mass SMBHs is not related with the morphology type of the host galaxies. We identify a moderate relation between  $R'$  and  $h_d/r_e$ . Objects with stronger radio emission tends to have larger bulge size. Our statistical analysis returns a correlation coefficient of  $r_s = -0.48$  at a significance level of  $2.47\sigma$  by adopting the Spearman rank-order statistics. The corresponding probability of null correlation is determined to be  $p_s = 0.0106$ . In addition, a correlation coefficient based on the Kendall’s  $\tau$  method is obtained to be  $\tau = -0.65$  at a significance level of  $2.41\sigma$ , which corresponds to a probability of null correlation of  $p_s = 0.0159$ .

## 4.2. Implications

One would argue that the powerful radio emission in the sample is emitted from star-forming regions in the host galaxies rather than from the AGNs (e.g., Kennicutt 1992). We estimate an upper limit of star formation rate (SFR) for each object through the calibration of  $\text{SFR} = 7.9 \times \frac{L_{[\text{OIII}]} / 10^{42} \text{erg s}^{-1}}{16.73 - 1.75[\log(\text{O}/\text{H}) + 12]} M_\odot \text{ yr}^{-1}$  in Kewley et al. (2004), by assuming the  $[\text{OII}]\lambda 3727$  line emission is fully contributed by the ongoing star formation.  $\log(\text{O}/\text{H}) + 12 = 9.2$  is the metallicity twice of the solar value that is usually used in AGNs (e.g., Ho 2005). With the estimated SFR, an upper limit of the radio power contributed by an underlying star formation  $P_{\text{exp}}$  is then inferred for each object by a combination of the relationship of  $\text{SFR}(M \geq 5M_\odot) = \frac{P_{\text{exp}, 1.4\text{GHz}}}{4.0 \times 10^{21} \text{W Hz}^{-1}} M_\odot \text{ yr}^{-1}$  in Condon (1992) and a Salpeter initial mass function. The bottom-left panel in Figure 6 shows the distribution of  $P_{\text{obs}}/P_{\text{exp}}$ , where  $P_{\text{obs}}$  is the observed radio power. The distribution indicates that the values of  $P_{\text{exp}}$  are typically lower than the observed ones by 1-2 orders of magnitudes, with the worst case of  $P_{\text{exp}} = 0.25P_{\text{obs}}$ .

Previous studies have reported two possible problems with the  $M_{\text{BH}}$  estimated from the  $M_{\text{BH}} - \sigma_*$  correlation for pseudo-bulges. The relationship of pseudo-bulge is either very weak (e.g., Kormendy et al. 2011) or shifted from that of classical bulge in both slope and intercept (e.g., Hu 2008; McConnell & Ma 2013; Ho & Kim 2014). These two problems have no essential effect on our results. At first, the values of  $M_{\text{BH}}$  listed in Table 1 are only representative in sample description and not directly involved in the revealed  $R' - n_B$  anti-

correlation. Secondly, compared to the relationship of pseudo-bulges, the  $M_{\text{BH}}$  estimated from the global relationship tends to be systematically over-estimated, rather than under-estimated, which in fact reinforces our sample selection of objects with small  $M_{\text{BH}}$ .

Both orientation and intrinsic mechanisms have been proposed to explain the powerful radio emission in AGNs with small  $M_{\text{BH}}$ . The orientation mechanism attributes the observed powerful radio emission to either a significant underestimation of  $M_{\text{BH}}$  due to a disk broad-line region (BLR) almost face-on (e.g., Baldi et al. 2016) or a boost in radio flux due to the beaming effect of a relativistic jet (e.g., Yuan et al. 2008; Liu et al. 2016 and references therein). In the intrinsic mechanism, the powerful radio emission can be ascribed to an energy extraction from either a disk wind (e.g., Blandford & Payne 1982; Wang et al. 2003; Cao 2016) or BH spin (e.g., Blandford & Znajek 1977).

The identified correlation between radio power and host bulge profile at first allows us to exclude the orientation scenarios for the current sample, simply because the bulge profile is not related with the orientation of either a disk BLR or a relativistic jet. In addition, our sample is selected on  $M_{\text{BH}}$  estimated from the  $M_{\text{BH}} - \sigma_*$  relation, which allows us to completely avoid the underestimation issue mentioned above.

We subsequently argue that the disk wind scenario is not applicable in the current sample, because our sample is selected on nuclear properties (i.e., accretion rate and  $M_{\text{BH}}$ ). In fact, a direct statistical analysis does not reveal any relation between  $R'$  and Eddington ratio  $\lambda_{\text{Edd}}$  assessed by  $\lambda_{\text{Edd}} \sim L_{[\text{OIII}]} / \sigma_*^4$  that is usually used in type II AGNs (e.g., Heckman & Best 2014).

With the exclusion of the three possible scenarios, we finally argue that the  $R' - n_{\text{B}}$  anti-correlation favors the scenario in which a low-mass SMBH is spun up by the gas accreted with significant disk-like rotational dynamics. An extraction of rotational energy of a BH plays an important role in launching powerful jets. The dependence of jet power on BH spin has been frequently suggested by various models (e.g., Ghosh & Abramowicz 1997; Wang et al. 2003), although the details depends on the adopted accretion disk model and the parametrization of the poloidal magnetic field. Both BH-BH merger and disk accretion can efficiently shape the final BH spin (e.g., Hughes & Blandford 2003; Volonteri et al. 2005). The revealed independence of  $R'$  on B/T ratio at first allows us to exclude the merger scenario for spinning-up the low-mass SMBHs.

A host rotational dynamics-related BH spinning-up is then suggested by the revealed  $R' - n_{\text{B}}$  correlation. A clear bulgeless disk with  $n_{\text{B}} \sim 1$  is recently discovered in 2MASX J23453268-0449256, an unique RL massive spiral galaxy with a powerful jet of a scale of  $\sim 1.6$  Mpc (Bagchi et al. 2014). In fact, BH spin is suggested to relate with host dynamics by a recent

theoretical study, in which a BH fueling flow attached to the dynamics of host galaxy at large scale is required to match the observed BH spin distribution well (Sesana et al. 2014). Observations indicate that the dynamics in pseudo-bulges is more dominated by rotation than in classical bulges (Kormendy & Kennicutt 2004). A low-mass SMBH can be efficiently spun up by the Bardeen-Peterson effect (Bardeen & Peterson 1975) that realign the BH-disk system through the interaction between the frame-dragging effect of the Lense-Thirring torque and the strong disk viscous stresses (e.g., King et al 2005; Perego et al 2009; Li et al 2015), if the gas accreted onto the SMBH has not only significant disk-like rotational dynamics, but also a mass exceeding the alignment mass limit of accretion event. The alignment mass limit is roughly  $m_{\text{align}} \sim a M_{\text{BH}} \sqrt{R_s/R_w}$  (Sikora et al. 2007), where  $a$  is the dimensionless angular momentum  $a = cJ/GM_{\text{BH}}^2$ , and  $R_s = 2GM_{\text{BH}}/c^2$  and  $R_w$  are the Schwarzschild radius and distance of wrap of the accretion disk, respectively. With the Eq. (22) in King et al. (2005) for  $R_s/R_w$ , the limit mass is reduced to  $m_{\text{align}} \propto a^{11/16} (L/L_{\text{Edd}})^{1/8} M_{\text{BH}}^{15/16}$ , which implies that, with respect to a high-mass one, a low-mass SMBH can be more readily spun up by a smaller mass increment.

Our results show that low-mass and high-mass SMBHs are spun up by two entirely different mechanisms that are believed to relate with two evolutionary paths. A pseudo-bulge that is favored by a spinning-up of low-mass SMBHs can be resulted from the secular evolution of disk galaxies (e.g, Silverman et al. 2011; Kormendy & Ho 2013; Kormendy & Kennicutt 2004; Fisher & Drory 2011), in which the pseudo-bulge might be related with either a second hump instability or a vertical dynamical resonance (e.g., Sellwood 2014). Meanwhile, a classical bulge favored for high-mass SMBHs is widely believed to be created through a “dry” merger of two galaxies (Toomre 1977), although this scenario is challenged by a recent identification of a RL and bulgeless spiral galaxy with a  $M_{\text{BH}} \sim 10^8 M_{\odot}$  (Bagchi et al. 2014).

## 5. CONCLUSION

We study the origin of spin of small SMBH on a sample of radio-selected nearby ( $z < 0.05$ ) Seyfert 2 galaxies with a  $M_{\text{BH}}$  of  $10^{6-7} M_{\odot}$ , which allows us to identify a new dependence of radio power on host bulge surface brightness. The dependence favors a scenario that a low-mass SMBH is spun up by the gas accreted with significant disk-like rotational dynamics.

The author would like to thank the anonymous referee for his/her very useful comments and suggestions for improving the manuscript. This study uses the SDSS archive data that was created and distributed by the Alfred P. Sloan Foundation. The study is supported



by the National Basic Research Program of China (grant 2009CB824800) and by National Natural Science Foundation of China under grants 11473036 and 11273027.

## REFERENCES

- Bagchi, J., Vivek, M., Vikram, V., et al. 2014, *ApJ*, 788, 18
- Bardeen, J. & Peterson, J. 1975, *ApJ*, 195, 65
- Becker, R. H., Helfand, D. J., White, R. L., Gregg, M. D., & Laurent-Muehleisen, S. A. 2003, *VizieR Online Data Catalog*, 8071
- Blandford, R. D., & Payne, D. G. 1982, *MNRAS*, 199, 883
- Blandford, R. D., & Znajek, R. L. 1977, *MNRAS*, 179, 433
- Cao, X. W. 2016, *astro-ph.HE/arXiv:1610.04061*, accepted by *ApJ*
- Chiaberge, M. & Marconi, A. 2011, *MNRAS*, 416, 917
- Coelho, P., Bruzual, G., Charlot, S., Weiss, A., Barbuy, B., & Ferguson, J. W. 2007, *MNRAS*, 328, 498
- Condon, J. J. 1992, *ARA&A*, 30, 575
- de Jong, R. S., Simard, L., Davies, R. L., Saglia, R. P., Burstein, D., Colless, M., McMahan, R., & Wegner, G. 2004, *MNRAS*, 355, 1155
- Fisher, D. B., & Drory, N. 2008, *ApJ*, 136, 773
- Fisher, D. B., & Drory, N. 2011, *ApJ*, 733, 47
- Ghosh, P. & Abramowicz, M. A. 1997, *MNRAS*, 292, 887
- Heckman, T. M., & Best, P. N. 2014, *ARA&A*, 52, 589
- Heckman, T. M., & Kauffmann, G. 2006, *New A Rev.*, 50, 677
- Heckman, T. M., Miley, G. K., van Breugel, W. J. M., & Butcher, H. R. 1981, *ApJ*, 247, 403
- Ho, L. C. 2005, *ApJ*, 629, 680
- Ho, L. C., & Kim, M. 2014, *ApJ*, 789, 17

- Hu, J. 2008, MNRAS, 386, 2242
- Hughes, S. A., & Blandford, R. D. 2003, ApJ, 585, 101
- Kaspi, S., Smith, P. S., Netzer, H., et al. 2000, ApJ, 533, 63
- Kennicutt, R. C. Jr. 1998, ARA&A, 36, 189
- Ker, L. M., Best, P. N., Rigby, E. E., Rttgering, H. J. A., & Gendre, M. A. 2012, MNRAS, 420, 2644
- Kewley, L. J., Dopita, M. A., Sutherland, R. S., Heisler, C. A., & Trevena, J. 2001, ApJ, 556, 121
- Kewley, L. J., Geller, M. J., & Jansen, R. A. 2004, AJ, 127, 2002
- Kewley, L. J., Groves, B., Kauffmann, G., & Heckman, T. 2006, MNRAS, 372, 961
- King, A. R., Lubow, S. H., Ogilvie, G. I., & Pringle, J. E. 2005, MNRAS, 363, 49
- Komossa, S., Voges, W., Xu, D. W., Mathur, S., Adorf, H., Lemson, G., Duschl, W. J., & Grupe, D. 2006, AJ, 132, 531
- Kormendy, J., Bender, R., & Cornell, M. E. 2011, Nature, 469, 374
- Kormendy, J. & Ho, L. C. 2013, ARA&A, 51, 511
- Kormendy, J., & Kennicutt, R. C. Jr. 2004, ARA&A, 42, 603
- Laor, A. 2000, ApJ, 543, 111
- Li, Y. R., Wang, J. M., Cheng, C., & Qiu, J. 2015, ApJ, 804, 45
- Liu, H., Wu, C., Wang, J., & Wei, J. Y. 2016, New A, 715, 113
- Magorrian, J. et al. 1998, AJ, 115, 2285.
- Mathur, S. 2000, MNRAS, 314, L17
- McConnell, N. J., & Ma, C. -P. 2013, ApJ, 764, 184
- Perego, A., Dotti, M., Colpi, M., & Volonteri, M. 2009, MNRAS, 399, 2249
- Richards, G. T., Fan, X. H., Newberg, H. J., et al. 2002, AJ, 123, 2945
- Sellwood, J. A. 2014, RvMP, 86, 1

- Sesana, A., Barausse, E., Dotti, M., & Rossi, E. M ApJ, 794, 104
- Sikora, M., Stawarz, ., Lasota, J. P. 2007, ApJ, 658, 815
- Silverman, J. D., et al. 2011, ApJ, 743, 2
- Simard, L., Willmer, C. N. A., Vogt, N. P., Sarajedini, V. L., Phillips, A. C., Weiner, B. J., Koo, D. C., Im, M. et al. 2002, ApJS, 142, 1
- Toomre, A. 1977, ARA&A, 15, 437
- Veilleux, S., & Osterbrock, D. E. 1987, ApJS, 63, 295
- Volonteri, M., Madau, P., Quataert, E., Rees, M. J. 2005, ApJ, 620, 69
- Wang, J. M., Ho, L. C., & Staubert, R. 2003, A&A, 409, 887
- Yuan, W., Zhou, H. Y., Komossa, S., Dong, X. B., Wang, T. G., Lu, H. L., & Bai, J. M. 2008, ApJ, 685, 801
- Zhou, H. Y., Wang, T. G., Yuan, W. M., Lu, H. L., Dong, X. B., Wang, J. X., & Lu, Y. J. 2006, ApJS, 166, 128

Table 1: Properties of the 30 radio-selected nearby ( $z < 0.05$ ) Seyfert 2 galaxies with small  $M_{\text{BH}}$ .

SDSS	$z$	$L_{[\text{OIII}]}$ $10^{40} \text{ erg s}^{-1}$	$P_{1.4\text{GHz}}$ $10^{21} \text{ W Hz}^{-1}$	$\log R'$	$\log(M_{\text{BH}}/M_{\odot})$	$D_n(4000)$	B/T	$h_d/r_e$	$n_{\text{B}}$
(1)	(2)	(3)	(4)	(5)	(6)	(7)	(8)	(9)	(10)
J005329.92-084604.0	0.0190	$20.37 \pm 0.15$	$5.68 \pm 0.12$	$-0.37 \pm 0.02$	6.84	1.37	$0.58 \pm 0.01$	$1.30 \pm 0.08$	$1.40 \pm 0.02$
J024703.64-003533.2	0.0423	$7.30 \pm 0.12$	$10.96 \pm 0.57$	$0.36 \pm 0.05$	6.72	1.47	$0.70 \pm 0.02$	$0.35 \pm 0.15$	$1.88 \pm 0.07$
J025329.59-001405.5	0.0288	$20.78 \pm 0.12$	$13.00 \pm 0.20$	$-0.02 \pm 0.02$	6.52	1.43	$0.54 \pm 0.03$	$2.24 \pm 0.44$	$1.62 \pm 0.05$
J073715.73+313110.9	0.0269	$13.44 \pm 0.05$	$3.30 \pm 0.22$	$-0.43 \pm 0.07$	7.00	1.74	$0.53 \pm 0.02$	$2.09 \pm 0.47$	$2.95 \pm 0.12$
J080547.34+225434.8	0.0304	$25.48 \pm 0.07$	$11.29 \pm 0.27$	$-0.17 \pm 0.02$	6.96	1.36	$0.26 \pm 0.01$	$3.30 \pm 0.34$	$1.04^{+0.06}_{-0.04}$
J082443.28+295923.5	0.0254	$28.77 \pm 0.18$	$2.56 \pm 0.21$	$-0.87 \pm 0.08$	6.78	1.30	$0.37 \pm 0.01$	$10.41 \pm 1.11$	$2.48 \pm 0.03$
J090613.76+561015.2	0.0466	$7.39 \pm 0.07$	$23.36 \pm 0.79$	$0.68 \pm 0.04$	6.90	1.26	$0.48 \pm 0.07$	$4.50 \pm 1.90$	$2.24 \pm 0.08$
J093236.58+095025.9	0.0489	$18.36 \pm 0.11$	$14.55 \pm 0.83$	$0.08 \pm 0.06$	6.83	1.39	$0.06 \pm 0.01$	$6.30 \pm 2.08$	$2.42 \pm 0.03$
J094044.50+211403.3	0.0244	$15.52 \pm 0.10$	$1.50 \pm 0.18$	$-0.84 \pm 0.12$	6.46	1.50	$0.24 \pm 0.01$	$2.02 \pm 0.23$	$3.06 \pm 0.08$
J095742.84+403315.8 <sup>a</sup>	0.0453	$7.26 \pm 0.08$	$10.58 \pm 0.65$	$0.34 \pm 0.06$	6.75	1.53	$0.35 \pm 0.02$	$1.87 \pm 0.32$	$1.00^{+0.01}_{-0.00}$
J112008.68+341845.8	0.0367	$6.34 \pm 0.08$	$2.60 \pm 0.41$	$-0.21 \pm 0.16$	6.66	1.53	$0.39 \pm 0.03$	$0.38 \pm 0.21$	$1.84 \pm 0.07$
J112135.17+042647.2	0.0470	$4.46 \pm 0.09$	$5.10 \pm 0.76$	$0.24 \pm 0.15$	6.63	1.49	$0.43 \pm 0.05$	$0.66 \pm 0.34$	$2.24 \pm 0.09$
J113630.49+265138.8 <sup>b</sup>	0.0333	$19.42 \pm 0.10$	$28.95 \pm 0.36$	$0.35 \pm 0.01$	6.42	1.37	$0.20 \pm 0.00$	$2.48 \pm 0.55$	$4.00 \pm 0.00$
J113808.01+111146.9 <sup>a</sup>	0.0357	$8.01 \pm 0.08$	$25.02 \pm 0.42$	$0.67 \pm 0.02$	6.87	1.48	$0.00 \pm 0.00$	.....	$1.00 \pm 0.00$
J114216.87+140359.7	0.0207	$20.16 \pm 0.07$	$1.76 \pm 0.13$	$-0.88 \pm 0.07$	6.29	1.51	$0.21 \pm 0.01$	$8.69 \pm 0.41$	$3.31 \pm 0.06$
J115429.40+425848.6	0.0235	$7.06 \pm 0.05$	$1.39 \pm 0.17$	$-0.53 \pm 0.13$	6.20	1.53	$0.26 \pm 0.01$	$5.19 \pm 0.55$	$2.59 \pm 0.16$
J122119.70+544923.2	0.0375	$9.59 \pm 0.08$	$9.72 \pm 0.46$	$0.19 \pm 0.05$	6.58	1.34	$0.80 \pm 0.04$	$2.54 \pm 0.57$	$3.48 \pm 0.19$
J122438.68+013243.0	0.0256	$6.54 \pm 0.06$	$1.81 \pm 0.23$	$-0.38 \pm 0.13$	6.84	1.43	$0.21 \pm 0.01$	$4.68 \pm 0.29$	$3.88 \pm 0.12$
J124054.96+080323.2 <sup>a</sup>	0.0478	$23.39 \pm 0.15$	$9.78 \pm 0.72$	$-0.20 \pm 0.07$	6.55	1.41	$0.28 \pm 0.06$	$0.61 \pm 0.20$	$1.00 \pm 0.00$
J140040.56-015518.2 <sup>b</sup>	0.0250	$25.54 \pm 0.12$	$3.78 \pm 0.21$	$-0.65 \pm 0.06$	6.69	1.19	$0.20 \pm 0.01$	$1.45 \pm 0.29$	$4.00^{+0.00}_{-0.01}$
J140804.00+071939.5	0.0238	$4.78 \pm 0.05$	$3.43 \pm 0.19$	$0.04 \pm 0.06$	6.13	1.26	$0.43 \pm 0.03$	$6.44 \pm 1.53$	$2.22 \pm 0.07$
J141041.34+133328.7	0.0162	$11.04 \pm 0.09$	$5.56 \pm 0.09$	$-0.12 \pm 0.02$	6.31	1.36	$0.37 \pm 0.01$	$4.96 \pm 0.21$	$3.10 \pm 0.10$
J151621.58+080604.7 <sup>a</sup>	0.0309	$14.66 \pm 0.14$	$31.12 \pm 0.29$	$0.51 \pm 0.01$	6.83	1.46	$0.28 \pm 0.01$	$0.40 \pm 0.18$	$1.00^{+0.03}_{-0.00}$
J153926.06+245636.8 <sup>a</sup>	0.0228	$11.96 \pm 0.06$	$10.22 \pm 0.17$	$0.11 \pm 0.02$	6.54	1.18	$0.39 \pm 0.01$	$1.58 \pm 0.06$	$1.00^{+0.02}_{-0.00}$
J154304.09+511248.9	0.0362	$14.68 \pm 0.10$	$7.77 \pm 0.41$	$-0.10 \pm 0.05$	6.16	1.30	$0.44 \pm 0.02$	$0.56 \pm 0.21$	$2.77 \pm 0.19$
J154559.09+270629.5	0.0314	$5.34 \pm 0.08$	$3.97 \pm 0.32$	$0.05 \pm 0.08$	6.47	1.49	$0.03 \pm 0.01$	$67.93 \pm 7.21$	$2.45 \pm 0.01$
J162451.25+192535.7	0.0359	$15.70 \pm 0.10$	$7.96 \pm 0.42$	$-0.16 \pm 0.05$	6.96	1.41	$0.49 \pm 0.02$	$2.73 \pm 0.62$	$1.99 \pm 0.06$
J163040.91+302919.4	0.0368	$16.83 \pm 0.12$	$6.74 \pm 0.44$	$-0.22 \pm 0.07$	7.02	1.56	$0.28 \pm 0.01$	$52.90 \pm 5.94$	$1.79 \pm 0.04$
J162622.65+210542.8	0.0320	$5.15 \pm 0.08$	$2.83 \pm 0.48$	$-0.08 \pm 0.17$	6.61	1.49	$0.21 \pm 0.01$	$3.09 \pm 0.66$	$2.65 \pm 0.04$
J215259.07-000903.4	0.0277	$30.59 \pm 0.05$	$1.74 \pm 0.17$	$-1.06 \pm 0.10$	7.01	1.71	$0.21 \pm 0.01$	$7.02 \pm 0.70$	$3.98 \pm 0.02$

<sup>a</sup>The Sersic index is fixed to be the minimum value of  $n_{\text{B}} = 1$  for the best-fit model.

<sup>b</sup>The Sersic index is fixed to be the maximum value of  $n_{\text{B}} = 4$  for the best-fit model.

Note. — Column (1): SDSS identification. Column (2): Redshift given by the SDSS spectroscopy pipelines. Column (3):  $[\text{OIII}]\lambda 5007$  line luminosity in unit of  $10^{40} \text{ erg s}^{-1}$ . Column (4): Radio power at 1.4GHz in unit of  $10^{21} \text{ W Hz}^{-1}$ . Column (5): Radio loudness  $R'$  calculated from Eq (1). Column (6): The BH mass estimated from the star light velocity dispersion  $\sigma_*$  through the well-established  $M_{\text{BH}} - \sigma_*$  relation. Column (7): Parameter of 4000Å break index defined as  $D_n(4000) = \int_{4000}^{4100} f_{\lambda} d\lambda / \int_{3850}^{3950} f_{\lambda} d\lambda$  (e.g., Coelho et al. 2007). Column (8): Bulge fraction obtained by 2-dimensional bulge+disk decompositions. Column (9): Ratio of the disk scale length over the bulge effective radius. Column (10): Modeled Sersic index. All the errors in Columns (7)-(9) are taken from the results reported by the GIM2D package that provides upper and lower limits of each free parameter at a confidence level of 99% based on the topology of the parameter space being built up in the fitting.

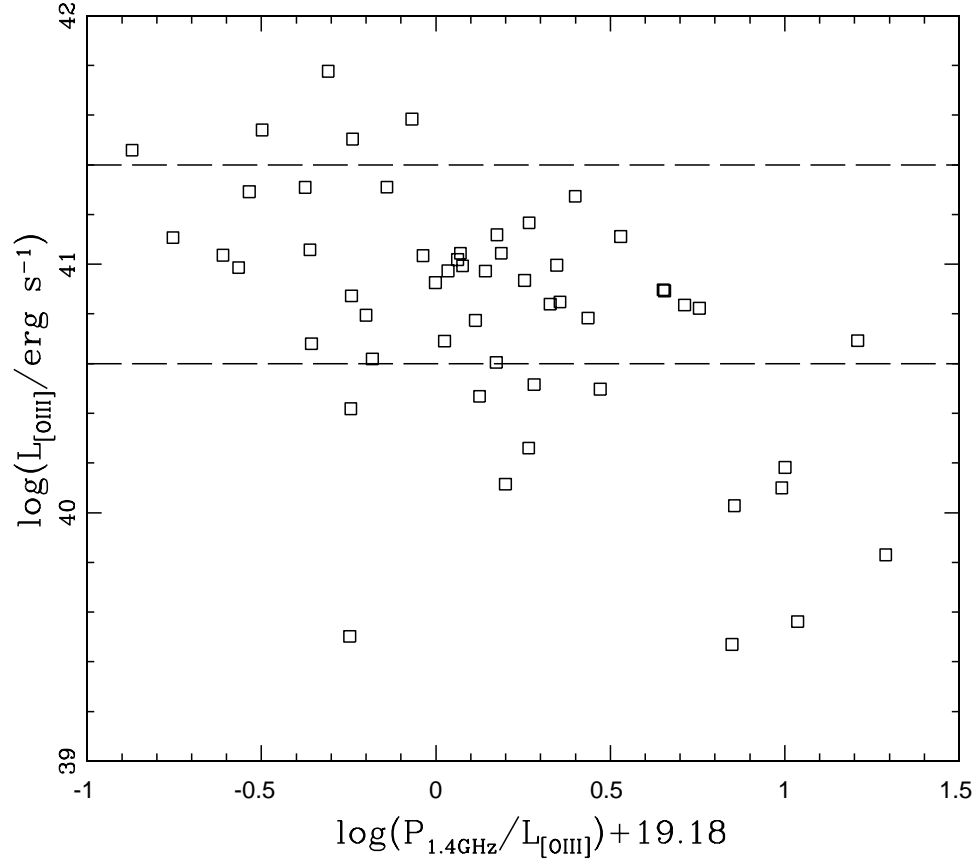


Fig. 1.— [O III] line luminosity plotted against the estimated radio loudness (see Eq. 1) for the 54 radio-selected nearby Seyfert 2 galaxies with small BH mass. In order to select a sample on AGN’s accretion property, only the 31 objects with  $L_{[\text{OIII}]}$  within the range (i.e.,  $\log L_{[\text{OIII}]} = 40.6 - 41.2$ ) marked by the two dashed lines are considered in our 2-dimensional bulge+disk decompositions.

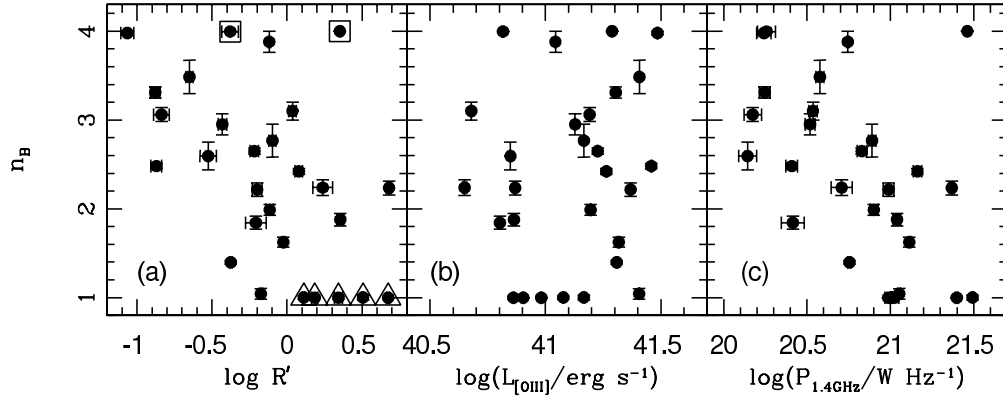


Fig. 2.— *Left panel:* An anti-correlation between the modeled Sersic index  $n_B$  and radio loudness  $R'$  estimated from Eq. (1). The objects with fixed value of  $n_B$  are marked by triangles for  $n_B = 1$  and by squares for  $n_B = 4$ . *Middle panel:*  $R'$  plotted against [O III] line luminosity. *Right panel:* The same as the middle one but for radio power at 1.4GHz.

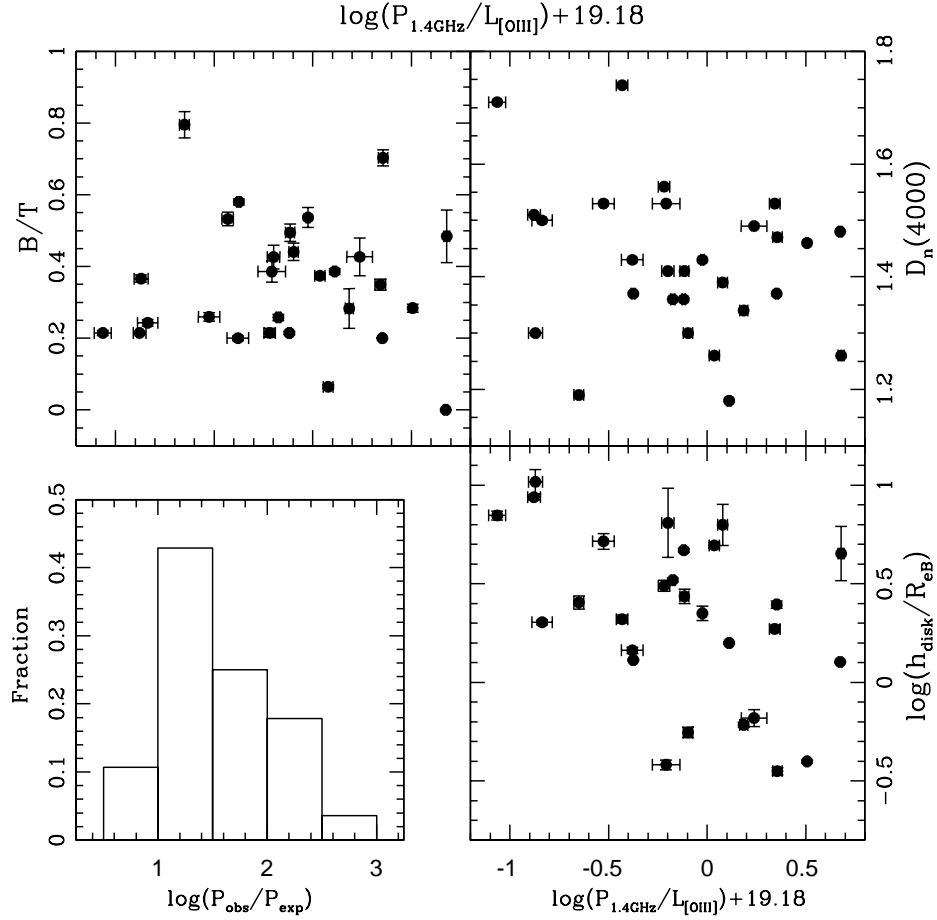


Fig. 3.— The estimated radio loudness is plotted as a function of bulge ratio  $B/T$  (top-left panel), host stellar population age  $D_n(4000)$  (top-right panel) and ratio of the disk scale length over the bulge effective radius  $h_d/r_e$  (bottom-right panel). The isolated panel at the bottom-left corner shows the distribution of the ratio of the observed radio power over the expected maximum contributed by underlying star formations.